Journal of
Mechanics of
Materials and Structures

DYNAMIC FATIGUE OF CRACKED PIEZOELECTRIC CERAMICS UNDER ELECTROMECHANICAL LOADING: THREE-POINT BENDING TEST AND FINITE ELEMENT ANALYSIS

Yasuhide Shindo, Fumio Narita and Mitsuru Hirama

Volume 4, Nº 4 April 2009

mathematical sciences publishers

JOURNAL OF MECHANICS OF MATERIALS AND STRUCTURES
Vol. 4, No. 4, 2009

DYNAMIC FATIGUE OF CRACKED PIEZOELECTRIC CERAMICS UNDER ELECTROMECHANICAL LOADING: THREE-POINT BENDING TEST AND FINITE ELEMENT ANALYSIS

YASUHIDE SHINDO, FUMIO NARITA AND MITSURU HIRAMA

This paper studies the dynamic fatigue or slow crack growth in piezoelectric ceramics under electromechanical loading by a combined numerical-experimental approach. Constant load-rate testing was conducted in three-point flexure using the single-edge precracked-beam specimens under zero and positive electric fields, and the effects of electric field and loading-rate on the fracture load and crack propagation were examined. A finite element analysis was also employed to calculate the energy release rate for the permeable, impermeable and open crack models, and the effect of electric field on the energy release rate was discussed. Crack propagation velocity versus energy release rate curves at various loading-rate were then estimated based on the finite element analysis using measured data.

1. Introduction

Piezoelectric ceramics of the lead zirconate titanate (PZT) class have been used for a number of years as sensors and actuators. The high mechanical stresses and intense electric fields in PZT ceramics can induce cracking that can lead to premature failure of the piezoelectric devices. The properties of PZT ceramics are also susceptible to degradation under electromechanical loading. Therefore, an understanding of piezoelectric fracture [Shindo et al. 2003; 2005] and fatigue [Cao and Evans 1994; Lynch et al. 1995] is a key issue for the efficient and reliable design of the piezoelectric devices. Shindo et al. [2007] conducted an experimental and analytical study of the static fatigue behavior of PZT ceramics under electromechanical loading. Narita et al. [2007] also reported experimental and numerical examination of the fatigue crack growth in PZT ceramics under a cyclic mechanical load and a constant electric field.

Certain environments may affect formation and extension of cracks over time and at stress levels well below that which causes immediate failure to occur. This process is called dynamic fatigue or slow crack growth. Slow crack growth parameters have been estimated for only a few commercial ceramics and glass, and no one has investigated the resistance of piezoelectric ceramics to slow crack growth and the influence of electric field on the dynamic fatigue behavior.

In this study, we report numerical and experimental examination of the dynamic fatigue or slow crack growth in piezoelectric ceramics under electromechanical loading. A crack was created normal to the poling direction. Constant load-rate testing was conducted in three-point flexure under zero and positive electric fields using single-edge precracked-beam method. A finite element analysis was also used to evaluate the energy release rate for the permeable, impermeable and open crack models, and the effect

Keywords: elasticity, finite element method, material testing, piezoelectric materials, dynamic fatigue, smart materials and structures.

Elastic stiffnesses ($\times 10^{10}$ N/m^2)					Piezoelectric coefficients (C/m^2)			Dielectric constants ($\times 10^{-10}$ C/Vm)	
c_{11}	c_{33}	c_{44}	c_{12}	c_{13}	e_{31}	e_{33}	e_{15}	ϵ_{11}	ϵ_{33}
17.0	16.5	3.05	10.6	11.5	−5.99	15.6	13.7	95.2	68.4

Table 1. Material properties of PCM-80.

of electric field on the energy release rate was discussed. The results were then examined in terms of the crack propagation velocity vs energy release rate curve.

2. Experimental procedure

Constant load-rate (dynamic fatigue) testing of commercially supplied hard PZT PCM-80 (Panasonic Electric Devices Co., Ltd., Japan) was carried out. The material properties are listed in Table 1. The specimens were 5 mm thick, 5 mm wide and 15 mm long. Poling was done along the axis of the 15 mm dimension. Through-thickness crack was introduced using the method described in [Narita et al. 2007]; the crack is about 0.5 mm long and has an initial gap of under 200 nm.

Figure 1 shows the testing set-up. A three-point flexure fixture with 13 mm span was used, and a load controlled mode was employed to apply for load rates from 0.05 to 1 Ns^{-1} under 0 and +0.1 MV/m. Crack growth was monitored during the test on the surface of the specimen with the aid of a digital microscope camera at 1000-fold magnification. The video camera records were also carefully observed to determine the crack length and the crack tip. From the detailed video photographs, the crack length can be easily measured. Because of the good resolution of the camera, the visual measurement of the crack length is not subject to large errors. This type of measurement procedure is used regularly. Due to cost and time constraints, the number of specimens was limited to two or three for each load-rate and electric field.

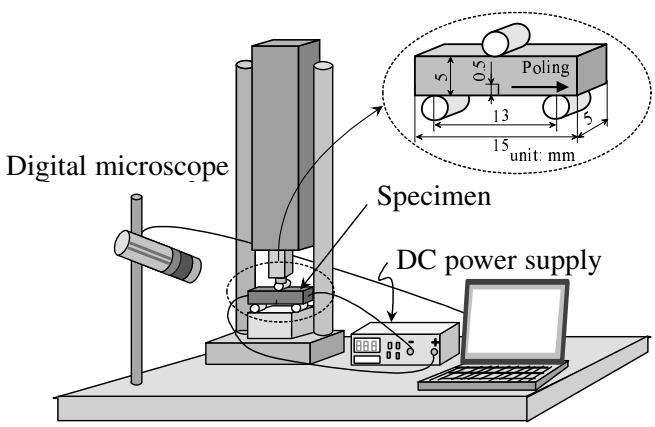

Figure 1. Testing set-up.

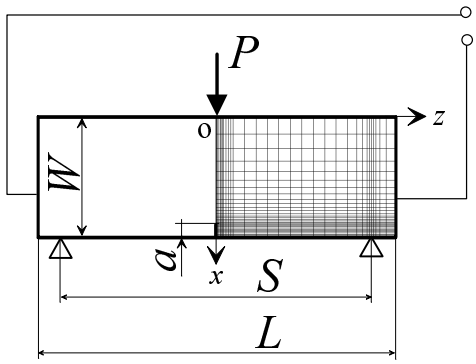

Figure 2. Schematic representation of finite element model.

3. Analysis

Consider a linear piezoelectric material with no body force and free charge. The basic equations for PZT ceramics, from [Tiersten 1969], are given in Appendix A.

Measured crack length a was recorded via video camera and then obtained as a function of the time t. In order to evaluate the energy release rate G of PZT, plane strain finite element analysis (ANSYS) was carried out for the cracked piezoelectric specimens. The specimen and loading geometries are shown in Figure 2. Let the coordinate axes $x = x_1$ and $z = x_3$ be chosen such that the $y = x_2$ axis coincides with the thickness direction. The z axis is oriented parallel to the poling direction. The three-point flexure specimen with a span S is a beam of width W and length L containing a crack of length a. Because of symmetry, only the right half of the model was used in the finite element analysis.

The crack is traction free and on its surface the normal component of the electric displacement and the tangential component of the electric field are continuous. Also, the geometry and the fields are symmetric. Thus

$$\sigma_{zx}(x, 0) = 0 \ (0 \le x \le W) \tag{1}$$

$$\begin{cases} u_z(x, 0) = 0 & (0 \le x \le W - a) \\ \sigma_{zz}(x, 0) = 0 & (W - a < x \le W) \end{cases} \tag{2}$$

$$\begin{cases} \phi(x, 0) = 0 & (0 \le x \le W - a) \\ E_x(x, 0) = E_x^c(x, 0) & (W - a < x \le W) \\ D_z(x, 0) = D_z^c(x, 0) & (W - a < x \le W) \end{cases} \tag{3}$$

where the superscript c stands for the electric quantity in the void inside the crack. Equations (3) constitute the permeable crack boundary conditions [Parton 1976; Shindo et al. 1990]. The electric potential is all zero on the symmetry planes inside the crack and ahead of the crack, so the boundary conditions of (3) reduce to $\phi(x, 0) = 0$ $(0 \le x \le W)$. The electric field intensity $E_x^c(x, 0)$ is equal to zero, and the electric displacement $D_z^c(x, 0)$ is determined precisely by $(3)_3$ with the electric permittivity of the vacuum $\epsilon_0 = 8.85 \times 10^{-12}$ C/Vm. A mechanical load is produced by the application of a prescribed force

P at $x = 0, z = 0$ along the x-direction. For electrical loads, a negative or positive electric potential $\phi_0/2$ is applied at the edge $0 \le x \le W$, $z = L/2$. Other boundary conditions are summarized below.
At $x = 0$ (top surface)

$$\sigma_{xx}(0, z) = -P\delta(z) \tag{4}$$
$$\sigma_{xx}(0, z) = 0 \quad (0 < z \le L/2) \tag{5}$$
$$\sigma_{xz}(0, z) = 0 \quad (0 \le z \le L/2) \tag{6}$$
$$D_x(0, z) = 0 \quad (0 \le z \le L/2) \tag{7}$$

At $z = L/2$ (side surface)

$$\sigma_{zz}(x, L/2) = 0 \quad (0 \le x \le W) \tag{8}$$
$$\sigma_{zx}(x, L/2) = 0 \quad (0 \le x \le W) \tag{9}$$
$$\phi(x, L/2) = \phi_0/2 \quad (0 \le x \le W) \tag{10}$$

At $x = W$ (bottom surface)

$$\sigma_{xx}(W, z) = 0 \quad (0 \le z < S/2, S/2 < z \le L/2) \tag{11}$$
$$u_x(W, S/2) = 0 \tag{12}$$

$$\sigma_{xz}(W, z) = 0 \quad (0 \le z \le L/2) \tag{13}$$
$$D_x(W, z) = 0 \quad (0 \le z \le L/2) \tag{14}$$

In Equation (4), $\delta(z)$ is the Dirac-delta function. The condition (10) gives the electric field $E_0 = -\phi_0/L$. In the finite element analysis, the energy release rate was computed using the path-independent integral approach. The energy release rate G is given by

$$G = \int_{\Gamma_0} \{Hn_x - (\sigma_{xx}u_{x,x} + \sigma_{zx}u_{z,x})n_x - (\sigma_{zx}u_{x,x} + \sigma_{zz}u_{z,x})n_z + D_xE_xn_x + D_zE_xn_z\}\mathrm{d}\Gamma \tag{15}$$

where Γ_0 is a contour closing a crack tip and n_x, n_z are the components of the outer unit normal vector. The electrical enthalpy density H is expressed as

$$H = \tfrac{1}{2}\{c_{11}(u_{x,x})^2 + c_{33}(u_{z,z})^2 + 2c_{13}u_{x,x}u_{z,z} + c_{44}(u_{x,z} + u_{z,x})^2\} - \tfrac{1}{2}\{\epsilon_{11}(E_x)^2 + \epsilon_{33}(E_z)^2\} - \{e_{15}(u_{x,z} + u_{z,x})E_x + (e_{31}u_{x,x} + e_{33}u_{z,z})E_z\}. \tag{16}$$

Equation (15) was implemented numerically in ANSYS using the J-integral approach, and the energy release rate was computed. For the calculation of J, three contours were defined in the finite element mesh. The values of J for each of these contours are practically identical and the variations with respect to the average value of J from three contours are less than 2%. Four-node element PLANE 13 was used in the model. The finite element mesh had 1900 elements and 1981 nodes. Our previous measurements of strain near electrode tip in piezoelectric devices [Yoshida et al. 2003; Shindo et al. 2004] and piezoelectric actuator tip deflection [Hayashi et al. 2003] verified the accuracy of the above scheme, and showed that the results obtained are of general applicability.

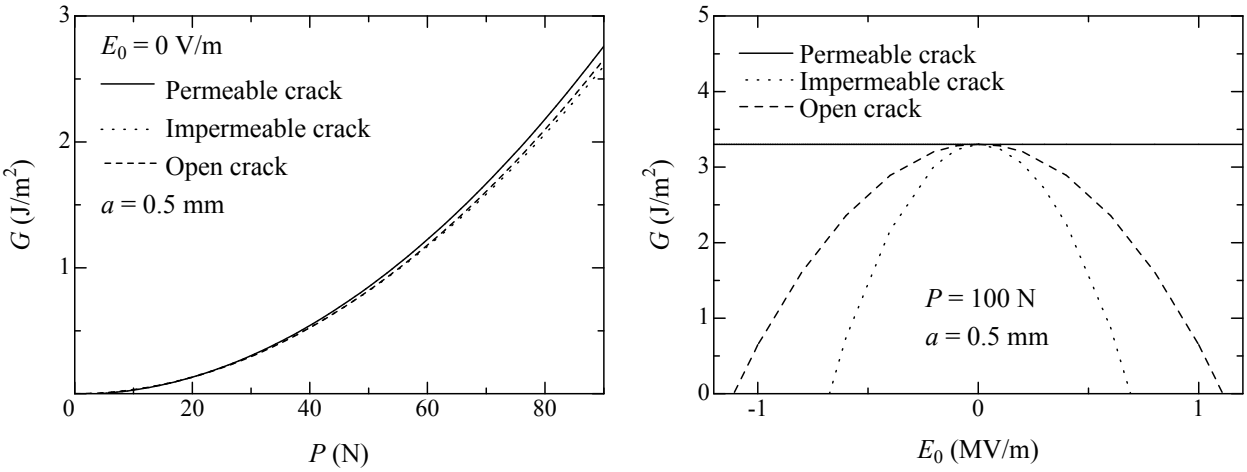

Figure 3. Left: Energy release rate versus applied load. Right: Energy release rate versus electric field.

McMeeking [2004] showed that due to a change of stored electrostatic energy within the crack, the energy release rate for an elliptical cavity of any shape is not equal to the energy release rate G for the slit-like crack as the material separates. Then he reported that if the initial crack gap is small, there is little difference between the energy release rate for the elliptical cavity and the G — see Equation (15) — for the slit-like crack. The energy release rates G for the impermeable [Deeg 1980; Pak 1990] and open [Hao and Shen 1994; McMeeking 1999] crack models are also discussed in Appendix B.

4. Results and discussion

Figure 3, left, presents the plot of the energy release rate G versus applied load P for the piezoelectric specimen (PZT PCM-80) with a crack of length $a = 0.5$ mm under electric field $E_0 = 0$ V/m. Little difference among three piezoelectric crack models is observed. Figure 3, right, shows the dependence of the energy release rate G for the permeable, impermeable and open crack models on the electric field E_0 under $P = 100$ N for $a = 0.5$ mm. The energy release rate for the permeable crack model is independent of the electric field. In the impermeable and open crack models, applying the electric field in either direction decreases the energy release rate. A negative energy release rate is also produced under large electric fields. According to the fracture mechanics interpretation, a negative energy release rate would correspond to a crack that could absorb energy due to crack extension. Since this would exclude the fracture in piezoelectric ceramics under electric fields, in contradiction with the experimental observations [Park and Sun 1995; Shindo et al. 2001, 2005], the parameters for the impermeable and open crack models have questionable physical significance. Therefore, the electrical boundary conditions (B.1) and (B.2) are not appropriate for a slit crack in piezoelectric ceramics, and the permeable crack model can be used to calculate the G of the specimens.

A summary of the results of constant load-rate testing for PZT PCM-80 under applied electric field $E_0 = 0$ and $+0.1$ MV/m is shown in Figure 4, where $\log P_c$ (fracture load) was plotted as a function of $\log(\mathrm{d}P/\mathrm{d}t)$ (load-rate). The error bars indicate maximum and minimum fracture loads at each load-rate

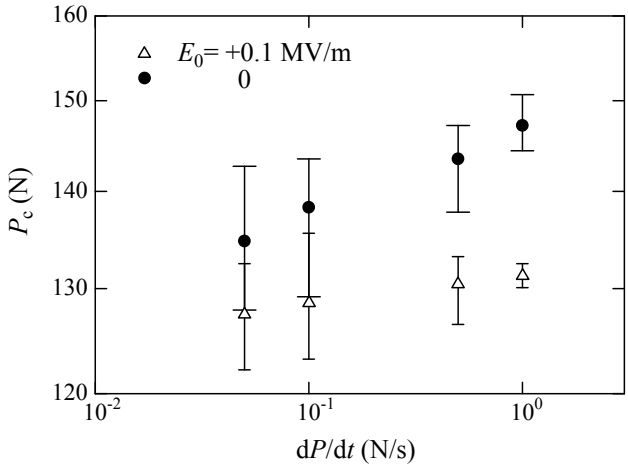

Figure 4. Fracture load as a function of load-rate.

and electric field, and triangle and dot are average values. The margin of error is larger at lower rates because of changes in microstructures near the crack tip at low load-rates. The PZT ceramics show an increase in fracture load as the load-rate increases, similar to behavior reported for dynamic fatigue in other non-piezoelectric ceramics [Pan et al. 1998; Choi and Salem 1998; Andrews et al. 2002]. The results also indicate that an overall decrease in fracture load occurs when testing under $E_0 = +0.1$ MV/m. Although experimental results show some scatter, the data are good enough to allow a relation between the fracture load and load-rate. The fracture load as a function of load-rate can be approximated by

$$P_c = K(\mathrm{d}P/\mathrm{d}t)^{1/(n+1)}, \tag{17}$$

where

$$\begin{aligned} &K = 147, \quad n = 34.6 \quad (E_0 = 0\ \text{V/m}), \\ &K = 131, \quad n = 99.5 \quad (E_0 = +0.1\ \text{MV/m}). \end{aligned} \tag{18}$$

Figure 5, left, shows typical curves of crack propagation, Δa, measured as a function of loading time t, under an electric field $E_0 = 0$ and $+0.1$ MV/m at load-rate of 1.0 N/s. The crack can be seen to grow at progressively decreasing growth rates, with increasing size only after a certain delay time, 50 s. The rate of crack growth of the specimen under $E_0 = +0.1$ MV/m is substantially greater than that under $E_0 = 0$ V/m. The final failure occurred when the total crack growth distance on the side surface under $E_0 = 0$ and $+0.1$ MV/m is about 159 and 184 μm, respectively. Note that the rate of crack growth does not depend on the electric field before 50 s of delay time. Figure 5, right, shows similar results at a load-rate of 0.05 N/s. The stable crack growth velocity occurs after a delay time of about 1600 s. The final failure occurred when the crack growth increment of the specimen under $E_0 = 0$ and $+0.1$ MV/m is about 91 and 171 μm, respectively.

Figure 6, left, shows a comparison of crack propagation velocities $\mathrm{d}a/\mathrm{d}t$ under $E_0 = 0$ and $+0.1$ MV/m at 1.0 N/s, plotted as a function of the energy release rate G. The crack propagation velocity is obtained by the experiment, whereas the energy release rate is calculated by the finite element analysis for the

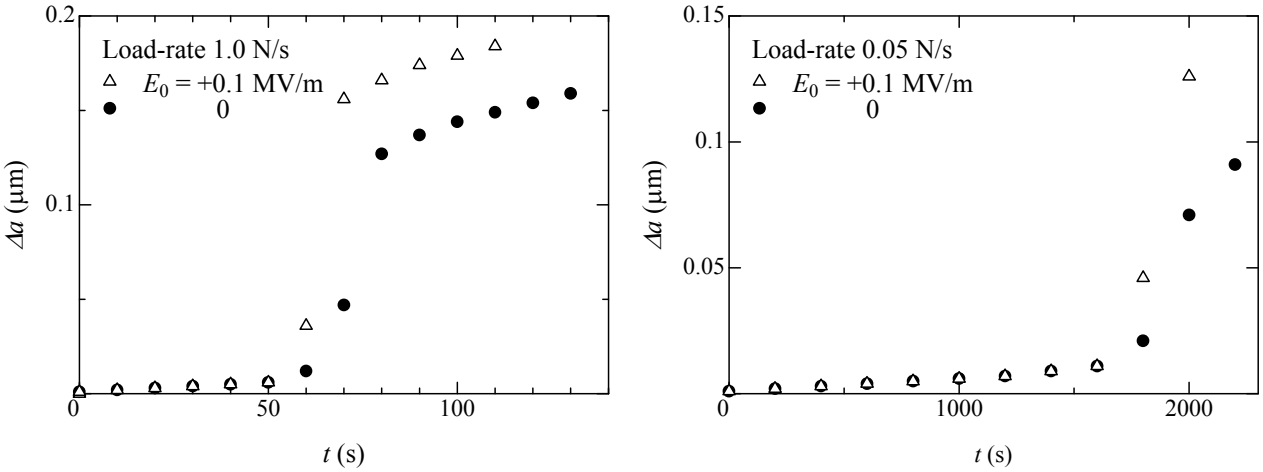

Figure 5. Variation of crack length as a function of time. Left: dP/dt=1.0 N/s. Right: dP/dt=0.05 N/s.

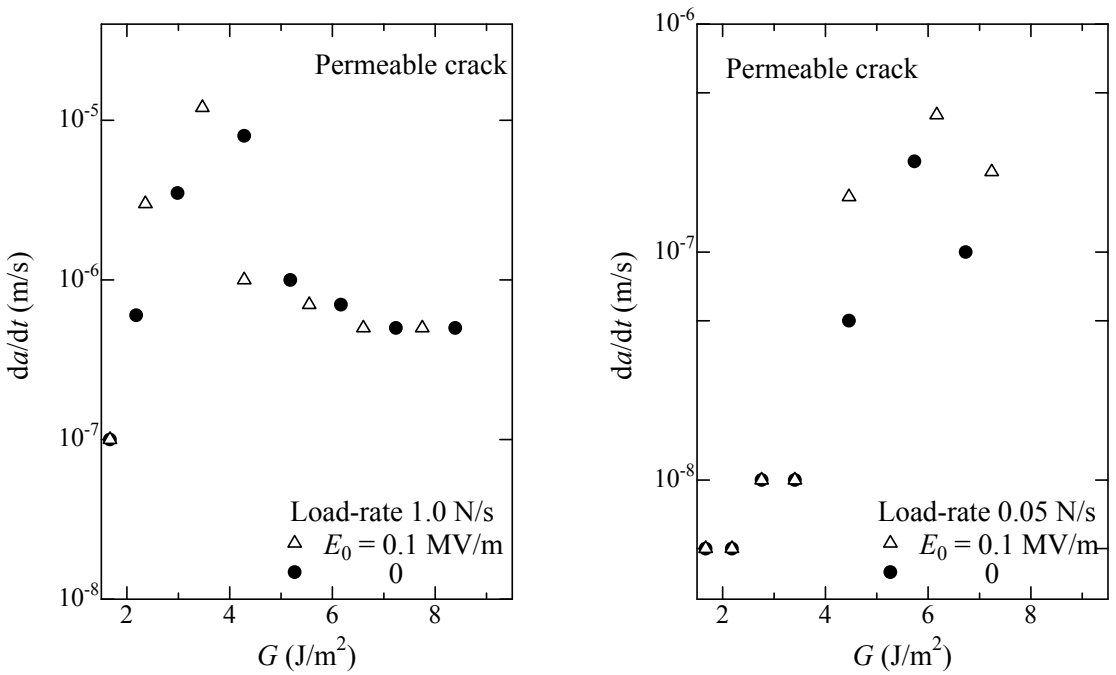

Figure 6. Crack propagation velocity as a function of energy release rate. Left: dP/dt=1.0 N/s. Right: dP/dt=0.05 N/s.

piezoelectric specimen with a permeable crack. The crack propagation velocity increases very quickly with the energy release rate, reaching a peak and then decreases before final failure. The decrease in the crack velocity is probably associated with microcrack nucleation and crack bridging [Lynch et al. 1995; Fang et al. 2004]. It can also been seen that positive electric field enhances crack propagation, whereas for $G > 5$ J/m^2, the crack velocity is not influenced by the electric field anymore. Figure 6, right, shows

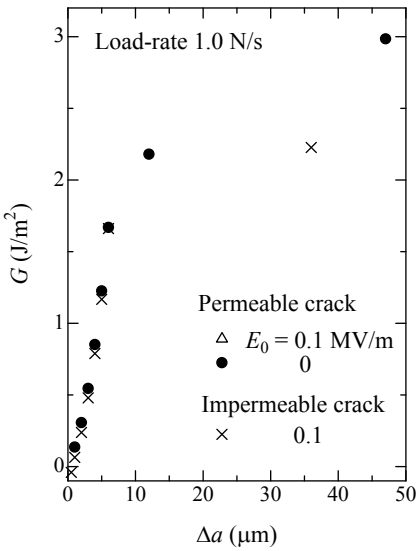

Figure 7. Energy release rate as a function of crack extension (dP/dt = 1.0 N/s).

similar results at load-rate of 0.05 N/s. The data suggest that there is a small influence of the electric field on the crack propagation for small G. At 0.05 N/s, the velocities are always lower than those at 1.0 N/s.

The energy release rate for the permeable crack model is calculated by the finite element analysis and plotted as a function of the measured crack extension under $E_0 = 0$ and $+0.1$ MV/m at 1.0 N/s in Figure 7. Also shown is the energy release rate for the impermeable crack model under $E_0 = +0.1$ MV/m. Comparing the energy release rates under $E_0 = 0$ MV/m for the permeable and impermeable crack models, little difference is observed (not shown). For the permeable crack model, the energy release rate increases with increasing the crack length and is independent of the electric field for small crack extensions. If we use the impermeable crack model to calculate the G, the energy release rate becomes negative (-0.04 J/m^2 for $\Delta a = 500$ nm) under $E_0 = +0.1$ MV/m and so, as mentioned earlier, we cannot use the impermeable crack model. Also, the energy release rate depends on the electric field for small crack extensions which is not in agreement with the experimental observations.

5. Conclusions

A combined numerical and experimental study is made to understand the influence of applied electric field on the crack behavior of piezoelectric ceramics. It is found that the piezoelectric ceramics under positive electric field has low dynamic fatigue or slow crack growth resistance, compared to those under no electric field. The crack propagation velocity increases at first with increasing the energy release rate, reaching a peak, and then tends to decrease at higher energy release rate before final failure. We expect the present study to encourage further research on the crack behavior of the piezoelectric ceramics under electromechanical loading.

Appendix A

The governing equations in Cartesian coordinates x_i $(i = 1, 2, 3)$ are

$$\sigma_{ji,j} = 0, \tag{A.1}$$

$$D_{i,i} = 0, \tag{A.2}$$

where σ_{ij} is the stress tensor, D_i is the electric displacement vector, $,i$ denotes partial differentiation with respect to the coordinate x_i, and the Einstein summation convention over repeated indices is used. The relation between the strain tensor ε_{ij} and the displacement vector u_i is

$$\varepsilon_{ij} = \tfrac{1}{2}(u_{j,i} + u_{i,j}). \tag{A.3}$$

The electric field intensity is

$$E_i = -\phi_{,i}, \tag{A.4}$$

where ϕ is the electric potential. The constitutive relations can be written as

$$\sigma_{ij} = c_{ijkl}\varepsilon_{kl} - e_{kij}E_k, \tag{A.5}$$

$$D_i = e_{ikl}\varepsilon_{kl} + \epsilon_{ik}E_k, \tag{A.6}$$

where c_{ijkl} and e_{ikl} are the elastic and piezoelectric constants, ϵ_{ik} is the dielectric permittivity, and

$$c_{ijkl} = c_{jikl} = c_{ijlk} = c_{klij}, \quad e_{kij} = e_{kji}, \quad \epsilon_{ik} = \epsilon_{ki}. \tag{A.7}$$

For piezoelectric ceramics which exhibit symmetry of a hexagonal crystal of class 6 mm with respect to the principal axes x_1, x_2, x_3, the constitutive relations can be written in the form

$$\begin{Bmatrix} \sigma_1 \\ \sigma_2 \\ \sigma_3 \\ \sigma_4 \\ \sigma_5 \\ \sigma_6 \end{Bmatrix} = \begin{bmatrix} c_{11} & c_{12} & c_{13} & 0 & 0 & 0 \\ c_{12} & c_{11} & c_{13} & 0 & 0 & 0 \\ c_{13} & c_{13} & c_{33} & 0 & 0 & 0 \\ 0 & 0 & 0 & c_{44} & 0 & 0 \\ 0 & 0 & 0 & 0 & c_{44} & 0 \\ 0 & 0 & 0 & 0 & 0 & c_{66} \end{bmatrix} \begin{Bmatrix} \varepsilon_1 \\ \varepsilon_2 \\ \varepsilon_3 \\ \varepsilon_4 \\ \varepsilon_5 \\ \varepsilon_6 \end{Bmatrix} - \begin{bmatrix} 0 & 0 & e_{31} \\ 0 & 0 & e_{31} \\ 0 & 0 & e_{33} \\ 0 & e_{15} & 0 \\ e_{15} & 0 & 0 \\ 0 & 0 & 0 \end{bmatrix} \begin{Bmatrix} E_1 \\ E_2 \\ E_3 \end{Bmatrix}, \tag{A.8}$$

$$\begin{Bmatrix} D_1 \\ D_2 \\ D_3 \end{Bmatrix} = \begin{bmatrix} 0 & 0 & 0 & 0 & e_{15} & 0 \\ 0 & 0 & 0 & e_{15} & 0 & 0 \\ e_{31} & e_{31} & e_{33} & 0 & 0 & 0 \end{bmatrix} \begin{Bmatrix} \varepsilon_1 \\ \varepsilon_2 \\ \varepsilon_3 \\ \varepsilon_4 \\ \varepsilon_5 \\ \varepsilon_6 \end{Bmatrix} + \begin{bmatrix} \epsilon_{11} & 0 & 0 \\ 0 & \epsilon_{11} & 0 \\ 0 & 0 & \epsilon_{33} \end{bmatrix} \begin{Bmatrix} E_1 \\ E_2 \\ E_3 \end{Bmatrix}, \tag{A.9}$$

where

$$\left.\begin{aligned} &\sigma_1 = \sigma_{11},\ \sigma_2 = \sigma_{22},\ \sigma_3 = \sigma_{33}, \\ &\sigma_4 = \sigma_{23} = \sigma_{32},\ \sigma_5 = \sigma_{31} = \sigma_{13},\ \sigma_6 = \sigma_{12} = \sigma_{21}, \end{aligned}\right\} \tag{A.10}$$

$$\left.\begin{aligned} &\varepsilon_1 = \varepsilon_{11},\ \varepsilon_2 = \varepsilon_{22},\ \varepsilon_3 = \varepsilon_{33}, \\ &\varepsilon_4 = 2\varepsilon_{23} = 2\varepsilon_{32},\ \varepsilon_5 = 2\varepsilon_{31} = 2\varepsilon_{13},\ \varepsilon_6 = 2\varepsilon_{12} = 2\varepsilon_{21}, \end{aligned}\right\} \tag{A.11}$$

$$\left.\begin{aligned} &c_{11} = c_{1111} = c_{2222},\ c_{12} = c_{1122},\ c_{13} = c_{1133} = c_{2233},\ c_{33} = c_{3333},\\ &c_{44} = c_{2323} = c_{3131},\ c_{66} = c_{1212} = \tfrac{1}{2}(c_{11} - c_{12}), \end{aligned}\right\} \tag{A.12}$$

$$e_{15} = e_{131} = e_{223},\quad e_{31} = e_{311} = e_{322},\quad e_{33} = e_{333}. \tag{A.13}$$

Appendix B

A solution procedure for the impermeable and open crack models is outlined here. The impermeable boundary condition becomes

$$\begin{aligned} \phi(x,0) &= 0 \quad (0 \le x \le W - a),\\ D_z(x,0) &= 0 \quad (W - a < x \le W). \end{aligned} \tag{B.1}$$

The energy release rate G for the impermeable crack model is given by Equation (15). The crack face electrical boundary condition for the open crack model is

$$\begin{aligned} \phi(x,0) &= 0 && (0 \le x \le W - a),\\ D_z^+ &= D_z^- && (W - a < x \le W),\\ D_z^+(u_z^+ - u_z^-) &= \epsilon_0(\phi^- - \phi^+) && (W - a < x \le W), \end{aligned} \tag{B.2}$$

where the superscripts $+$ and $-$ denote, respectively, the right and left sides of the cross-section where the crack is located (see Figure 2). The open crack model calculations start with $\phi = 0$ on the crack surface [McMeeking 1999]. The crack opening displacement and electric displacement on the crack surface are estimated, and the resulting potential difference is applied to the crack surface. The electroelastic fields are again solved leading to new crack opening displacement and electric displacement on the crack surface. If this is accomplished, then the potential difference is applied once more to the crack surface. The process is repeated until the solution converges. The energy release rate G for the open crack model is obtained by Equation (15).

Acknowledgements

This work was partially supported by a Grant-in-Aid for Scientific Research (B) from the Ministry of Education, Culture, Sports, Science and Technology, Japan.

References

[Andrews et al. 2002] M. J. Andrews, M. K. Ferber, and E. Lara-Curzio, "Mechanical properties of zirconia-based ceramics as functions of temperature", *J. Eur. Ceram. Soc.* **22**:14–15 (2002), 2633–2639.

[Cao and Evans 1994] H. C. Cao and A. G. Evans, "Electric-field-induced fatigue crack growth in piezoelectrics", *J. Am. Ceram. Soc.* **77**:7 (1994), 1783–1786.

[Choi and Salem 1998] S. R. Choi and J. A. Salem, "'Ultra'-fast fracture strength of advanced ceramics at elevated temperatures", *Mater. Sci. Eng. A* **242**:1–2 (1998), 129–136.

[Deeg 1980] W. F. J. Deeg, *The analysis of dislocation, crack, and inclusion problems in piezoelectric solids*, Ph.D. thesis, Stanford University, 1980.

[Fang et al. 2004] D. Fang, B. Liu, and C. T. Sun, "Fatigue crack growth in ferroelectric ceramics driven by alternating electric fields", *J. Am. Ceram. Soc.* **87**:5 (2004), 840–846.

[Hao and Shen 1994] T. H. Hao and Z. Y. Shen, "A new electric boundary condition of electric fracture mechanics and its applications", *Eng. Fract. Mech.* **47**:6 (1994), 793–802.

[Hayashi et al. 2003] K. Hayashi, Y. Shindo, and F. Narita, "Displacement and polarization switching properties of piezoelectric laminated actuators under bending", *J. Appl. Phys.* **94**:7 (2003), 4603–4607.

[Lynch et al. 1995] C. S. Lynch, W. Yang, L. Collier, Z. Suo, and R. M. McMeeking, "Electric field induced cracking in ferroelectric ceramics", *Ferroelectrics* **166**:1 (1995), 11–30.

[McMeeking 1999] R. M. McMeeking, "Crack tip energy release rate for a piezoelectric compact tension specimen", *Eng. Fract. Mech.* **64**:2 (1999), 217–244.

[McMeeking 2004] R. M. McMeeking, "The energy release rate for a Griffith crack in a piezoelectric material", *Eng. Fract. Mech.* **71**:7–8 (2004), 1149–1163.

[Narita et al. 2007] F. Narita, Y. Shindo, and F. Saito, "Cyclic fatigue crack growth in three-point bending PZT ceramics under electromechanical loading", *J. Am. Ceram. Soc.* **90**:8 (2007), 2517–2524.

[Pak 1990] Y. E. Pak, "Crack extension force in a piezoelectric material", *J. Appl. Mech.* (*ASME*) **57**:3 (1990), 647–653.

[Pan et al. 1998] L. S. Pan, M. Matsuzawa, and S. Horibe, "Stress rate dependence of fracture strength in pre-cracked zirconia ceramics", *Mater. Sci. Eng. A* **244**:2 (1998), 199–206.

[Park and Sun 1995] S. B. Park and C. T. Sun, "Fracture criteria for piezoelectric ceramics", *J. Am. Ceram. Soc.* **78**:6 (1995), 1475–1480.

[Parton 1976] V. Z. Parton, "Fracture mechanics of piezoelectric materials", *Acta Astronaut.* **3**:9–10 (1976), 671–683.

[Shindo et al. 1990] Y. Shindo, E. Ozawa, and J. P. Nowacki, "Singular stress and electric fields of a cracked piezoelectric strip", *Int. J. Appl. Electrom. Mater.* **1** (1990), 77–87.

[Shindo et al. 2001] Y. Shindo, M. Oka, and K. Horiguchi, "Analysis and testing of indentation fracture behavior of piezoelectric ceramics under an electric field", *J. Eng. Mater. Technol.* (*ASME*) **123**:3 (2001), 293–300.

[Shindo et al. 2003] Y. Shindo, F. Narita, K. Horiguchi, Y. Magara, and M. Yoshida, "Electric fracture and polarization switching properties of piezoelectric ceramic PZT studied by the modified small punch test", *Acta Mater.* **51**:16 (2003), 4773–4782.

[Shindo et al. 2004] Y. Shindo, M. Yoshida, F. Narita, and K. Horiguchi, "Electroelastic field concentrations ahead of electrodes in multilayer piezoelectric actuators: experiment and finite element simulation", *J. Mech. Phys. Solids* **52**:5 (2004), 1109–1124.

[Shindo et al. 2005] Y. Shindo, F. Narita, and M. Mikami, "Double torsion testing and finite element analysis for determining the electric fracture properties of piezoelectric ceramics", *J. Appl. Phys.* **97** (2005), 114109.

[Shindo et al. 2007] Y. Shindo, F. Narita, and F. Saito, "Static fatigue behavior of cracked piezoelectric ceramics in three-point bending under electric fields", *J. Eur. Ceram. Soc.* **27**:10 (2007), 3135–3140.

[Tiersten 1969] H. F. Tiersten, *Linear piezoelectric plate vibrations*, Plenum, New York, 1969.

[Yoshida et al. 2003] M. Yoshida, F. Narita, Y. Shindo, M. Karaiwa, and K. Horiguchi, "Electroelastic field concentration by circular electrodes in piezoelectric ceramics", *Smart Mater. Struct.* **12**:6 (2003), 972–978.

Received 8 Nov 2007. Revised 1 Aug 2008. Accepted 11 Aug 2008.

YASUHIDE SHINDO: shindo@material.tohoku.ac.jp
Department of Materials Processing, Graduate School of Engineering, Tohoku University, Sendai 980-8579, Japan

FUMIO NARITA: narita@material.tohoku.ac.jp
Department of Materials Processing, Graduate School of Engineering, Tohoku University, Sendai 980-8579, Japan

MITSURU HIRAMA: *Department of Materials Processing, Graduate School of Engineering, Tohoku University, Sendai 980-8579, Japan*